A holistic Approach on the Simulation of Rotary-Friction-Welding

D. Schmicker[1], K. Naumenko[1] and J. Strackeljan[1]

[1] Otto-von-Guericke Universität Magdeburg, Universitätsplatz 2, 39106 Magdeburg, Germany

E-mail: david.schmicker@ovgu.de

Abstract

The contribution deals with a new holistic approach on the process simulation of Rotary Friction Welding (RFW). The main focus in this regard is on the proper determination of process parameters for new pairs of weld partners in a complete virtual manner. Basis of the simulation is a Carreau fluid material law coupled with the heat transfer problem. The plastic deformations of the flash are mapped by Lagrangian formulated finite elements involving sophisticated remeshing procedures in order to avoid spurious element distortions. A penalty contact approach in conjunction with a regularized Coulomb friction law is able to predict the interface forces in a very robust way. A self-written code is capable of simulating the whole process in adequate computation times, taking advantage of the general axial symmetry of the problem. After summarized derivation of the governing equations and the utilized material, a practical example is considered in order to demonstrate the performance of the model. A qualitative comparison of the flash shape with an experimental sample and an exemplary influence study of the process parameters conclude the paper.

Introduction

The process of Rotary Friction Welding (RFW) is a solid state welding process, being applied to a vast field of applications from automotive industry, railway industry up to aeronautics [6], [7]. Main benefits of RFW are the process stability, the high-quality joints and the good potential for process automation. Moreover, the range of weldable materials is much wider, while neither additives nor filler material are necessary for joining.

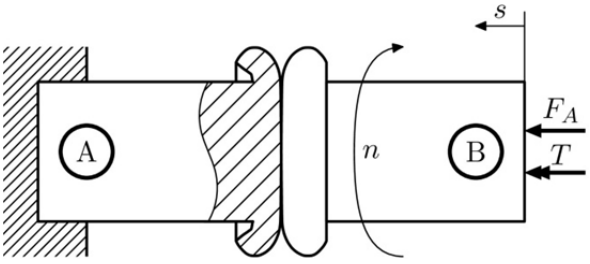

Figure 1: The main process parameter of RFW.

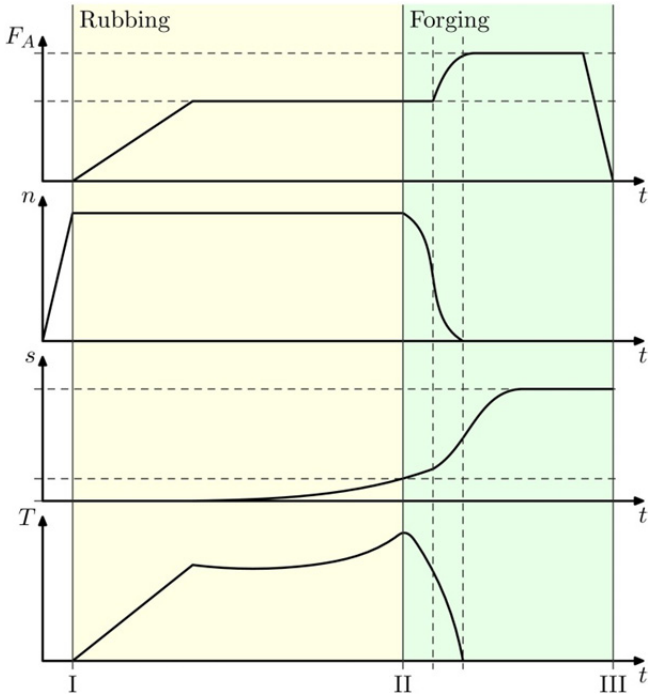

Figure 2: Typical process parameter runs at RFW.

Whereas at conventional welding processes the liquid phase of the material is usually reached, RFW does not exceed the melting temperature of each of the welding parts giving rise for a smaller heat affected zone [17]. Besides RFW also other friction welding processes coexist like Linear Friction Welding (LFW), Friction Stir Welding (FSW) and Orbital Friction Welding (OFW), for instance, differing mainly in the relative movement direction of the two welded parts. However, the physics of joining remain similar since the binding mechanism for all of them is material diffusion under high temperature and pressure. Already back in the 1970's research groups investigated the driving physical phenomena of RFW being heat generation, heat conduction, plastic deformation, abrasion of the friction surfaces and the material diffusion [17]. Ever since the main ambition therein is the prediction of stable, cycle time minimizing sets of process parameter. In Figure 1 a schematic illustration of the RFW process is given, highlighting the main process measures being the axial feed $s(t)$, the axial force $F_A(t)$, the torque $T(t)$ and the rotary speed $n(t)$. In accordance with the drive of the machine, one can distinguish between Inertia Friction Welding (IFW) and Direct-Drive

Friction Welding (DDFW). The first procedure utilizes the stored energy of a fly wheel for friction generation, whereas the DDFW process is continuously driven. Concerning DDFW the simplest form of process control is force driven, which means that the rotary speed and axial force are given in dependence of the time, and the torque and feed are determined by the physics of the weld. During the process it is usually distinguished between the rubbing (I-II) and the forging stage (II-III) as displayed in Figure 2. Typical weld parameters are the friction and forging force, the friction time, the rotary speed and the kind of breaking the spindle. In order to optimize these parameters and the process control it is inevitable to understand the physical phenomena of the process. The models found in the literature can generally be divided in pure thermal and coupled thermo-mechanical ones. Representatives of the first group focus rather on predicting the temperature profiles in friction welds as in [3], [5], [14], whereas the mechanically coupled approaches can be categorized in Computational Solid Mechanics (CSM) models and Computational Fluid Dynamics (CFD) models. Members of CSM are Hamilton et al. [11] and Schmidt et al. [18], for instance. Main feature of these kinds of models is that small deformations are incorporated and, hence, effects like residual stresses and thermal expansions can be accounted for. Mostly, a Johnson-Cook material law is assessed as a basis for the dependency of the yield stress on the elastic strains, the plastic strain rate and the temperature [13]. A certain drawback of CSM models is that the computational expense is likely to be higher than compared to CFD models. The latter modeling technique treats the kneadable phase of a material as a fluid with very high viscosity, which is a favorable approach in the field of computational plasticity [9]. The material behavior in this regard is primarily described by the underlying function of the dynamic viscosity on the strain rate and temperature. In fitting the corresponding curves to experimental data several suggestions can be found in literature. The two most common approaches therein are the Norton power approach [4] , [15] and the Garofalo creep law [8], also often referred to as Sheppard-Wright viscosity law [1], [12], [16], [21]. Besides pure CSM and CFD models also combined procedures exist, enabling the residual stresses computation by staging the simulation into a CSM and a CFD part [10], [19].

In the present contribution a fully-coupled, thermo-mechanical CFD model for the simulation of a DDFW process is illustrated. The fluid law is based on a Norton power approach, wherein the temperature dependency is incorporated by a Johnson-Cook law. In order to ensure physical behavior when reaching the liquid phase and for the sake of avoiding numerical problems at small loads the material law is formulated in terms of a Carreau fluid [2]. Main benefit of the given representation of the material law is that even without experimental knowledge about the viscosity data of the material, the plastic flow behavior can be assessed by easy accessible parameters like the yield limit at room temperature and the melt temperature.

The presented model is encapsulated in an in-house finite element code called *virtua RFW*. It features automatic meshing and remeshing algorithms of the Lagrange formulated elements, penalty contact algorithms, an augmented Lagrange method for keeping the volume constraint of the plastic flow, and an adaptive time step solver, enabling a robust and efficient simulation of DDFW.

The paper is structured as follows: First, the suggested fluid law is illustrated and the basic governing equations in simulating DDFW are given. Secondly, qualitative example problems are given, highlighting the capabilities of the presented modeling approach. A comprehension of the main findings concludes the paper.

Modeling of the process

The presented model bases upon a fully temperature-coupled fluid law for mapping the flash formation and the heat flux in the component parts. Involving the strain rate tensor $\boldsymbol{D}$ and the effective viscosity μ the deviatoric stresses are given by

$$\boldsymbol{s} = 2\mu\,\mathrm{dev}(\boldsymbol{D}). \tag{1}$$

Involving the von Mises strain rate $\dot{\varepsilon}_{vM} = \sqrt{2/3\boldsymbol{D}\cdot\cdot\boldsymbol{D}}$ the effective viscosity is assessed by the Carreau fluid law

$$\mu = \left[1 + \left(\left(\frac{\sigma_0}{3\dot{\varepsilon}_0\mu_0}\right)^{\frac{n}{1-n}} \frac{\dot{\varepsilon}_{vM}}{\dot{\varepsilon}_0}\right)^2\right]^{\frac{1-n}{2n}} (\mu_0 - \mu_\infty) + \mu_\infty. \tag{2}$$

Therein, the material constants are the initial viscosity μ_0 , being rather a numerical parameter for curing the singularity at low loads, the saturation viscosity μ_∞ , which can be interpreted as viscosity of the liquid phase, the Norton exponent n ranging usually between 3…10 [4] and the temperature dependent yield stress σ_0. For the yield stress either temperature tabulated data or the Johnson-Cook approach

$$\sigma_0(\Theta) = \begin{cases} \sigma_{0,R}\left[1 - \left(\frac{\Theta-\Theta_R}{\Theta_M-\Theta_R}\right)^m\right], & \Theta < \Theta_M \\ 0, & \Theta \geq \Theta_M \end{cases} \tag{3}$$

may be taken into account, involving the yield stress $\sigma_{0,R}$ at room temperature Θ_R , the material's melting point Θ_M , a reference strain rate $\dot{\varepsilon}_0$ being able to be chosen 1.0s^{-1} and the exponent m which usually is in between 0.5 and 1.5 [13]. In Figure 3 the viscosity dependency of eq. (2) is illustrated on the basis of a certain set of material parameters.

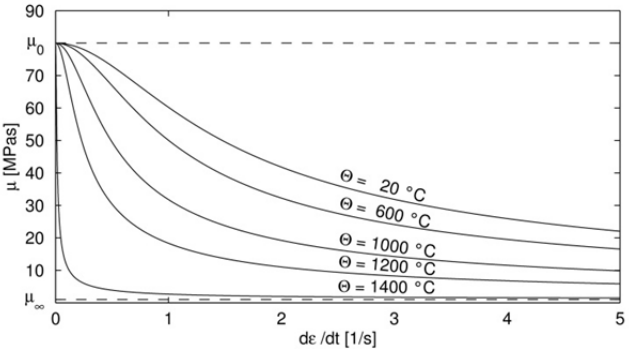

Figure 3: Viscosity – strain rate dependency of the presented Carreau fluid law.

Applying the material law on a one-dimensional stress state yields the stress – strain rate dependencies displayed in Figure 4. A major benefit of the presented material law is that the material behavior is mainly determined by the melting temperature and the yield limit at room temperature, which are usually easy accessible parameters. The exponents n and m can take some standard values for a coarse assessment of the simulation.

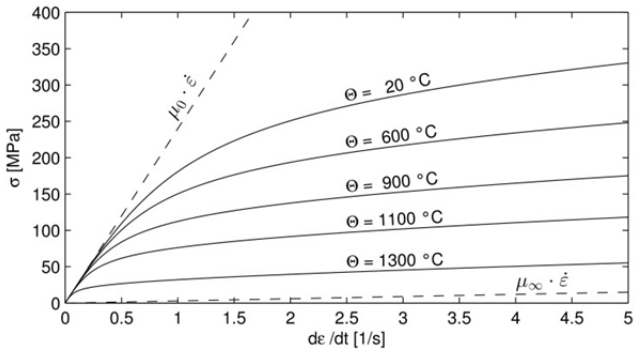

Figure 4: Stress – strain rate curves of the presented Carreau fluid law.

On the other hand, due to the limit viscosities μ_0 and μ_∞ the solution of the system equations is very robust and even solvable if loads are low or temperatures get near the melting point. The simulation bases upon the solution of the balance of linear momentum which is

$$\mathrm{div}(\boldsymbol{\sigma}) = 0. \tag{4}$$

In eq. (4) the inertia forces and body forces are neglected, which is admissible since they are subordinate at the process of RFW. The pressure part of Cauchy's stress tensor $\boldsymbol{\sigma}$ is accounted for an Augmented Lagrange strategy. The energy balance is stated as

$$\rho\, c\, \dot{\Theta} = -\mathrm{div}(\boldsymbol{q}) + \boldsymbol{\sigma} \cdot\cdot \boldsymbol{D} \tag{5}$$

with the mass density ρ, the heat capacity c and the heat flux $\boldsymbol{q}$. The inner body heat flux is assessed by Fourier's heat conduction law

$$\boldsymbol{q} = -\kappa_c\, \mathrm{grad}(\Theta) \tag{6}$$

involving the heat conductivity κ_c, while the heat flux across the boundary is

$$\boldsymbol{q} = \alpha_{surf}(\Theta - \Theta_\infty)\boldsymbol{n} + r_q\, \boldsymbol{n} \tag{7}$$

with the heat transport coefficient α_{surf}, the frictional heat source r_q and the surface normal vector $\boldsymbol{n}$. The pressure p at the contact surface in between the two work pieces is mapped by a penalty contact law. It is linked to the frictional shear forces by

$$\tau_{\varphi\varphi} = \frac{2\eta p}{\pi} \arctan\left(\frac{\Delta v_\varphi}{a_{reg}}\right) \tag{8}$$

taking the temperature-dependent friction coefficient η , the velocity difference of the contact interfaces Δv_φ and a regularization parameter a_{reg} into account. Thus, the heat source at the rubbing interface is

$$r_q = \tau_{\varphi\varphi} \Delta v_\varphi. \tag{9}$$

The spatial discretization of the domain is performed by 6-noded Lagrange formulated finite elements, as suggested in [15] and [20], for instance. The element formulation is 2.5D, meaning that a two-dimensional, axisymmetric domain is meshed while each node obtains three displacement degrees of freedom enabling the twist of the weld. Sophisticated remeshing procedures based on Delaunay-triangulation are capable of mapping the large deformations during the process. Both, the mechanic and the thermodynamic subproblem, are integrated on the same time grid, by first order accurate finite differences. An adaptive time step control algorithm enables a robust and efficient simulation of the RFW process. The presented model is programmatically conducted within Matlab by a self-written finite element code called *virtua RFW*. To this end, it supports a stable and efficient simulation of the friction welding process of similar parts, assuming symmetry between the rotary and stationary component part.

Results

Subsequently, the model performance will be demonstrated on a concrete friction weld example of two similar parts. Qualitative validation of the simulation results is achieved by comparison of the weld parameters and flash shapes with a sample being welded on the friction welding machine RH-800-SE illustrated in Figure 4.

Figure 4: Friction welding machine RH-800-SE constructed by H&B Omega Europa GmbH Magdeburg.

The geometry of the welded parts and the material parameters of the construction steel S235 are summed up in Table 1. Therein, the exponents m and n as well as the viscosities μ_0 and μ_∞ are estimated values and have not been experimentally validated. Same holds for the friction coefficient η which is assumed to be constant. Although it is obvious that through these assumptions only qualitative simulation re-

sults are to be expected, the simulation gives significant insights in the physics of the welding process and is able to illustrate the dependence of the process parameter on the flash shape, for instance. During the simulation symmetry of the weld partners has been assessed, cutting the computational effort to the half. This step is generally admissible if similar welds are observed, inertia forces are neglected and the heat transport coefficient α_{surf} does not depend on the rotary speed.

TABLE 1: GEOMETRY AND MATERIAL OF THE WELD

Reference yield limit $\sigma_{0,R}$	235 $\frac{N}{mm^2}$
Johnson Cook exponent m	1.3
Reference strain rate $\dot{\varepsilon}_0$	1 s^{-1}
Norton exponent n	10
Melt temperature Θ_M	1420°C
Room temperature Θ_R	20°C
Viscosity μ_0	10^8 MPas
Viscosity μ_∞	10^{-2} MPas
Mass density ρ	7.85 $\frac{g}{cm^3}$
Heat capacity c	460 $\frac{J}{kgK}$
Heat conductivity κ_c	50 $\frac{W}{mK}$
Heat transport coefficient α_{surf}	100 $\frac{W}{m^2K}$
Friction coefficient eta	0.2
Outer diameter d_a	80 mm
Inner diameter d_i	64 mm

TABLE 2: PARAMETER SETS OF WELDING

	Set A	Set B
Rubbing duration t_{I-II}	12 s	4.3 s
Rubbing force $F_{A,I-II}$	50 kN	50 kN
Forging duration t_{II-III}	3s	7s
Forging force $F_{A,II-III}$	110 kN	110 kN
Rotary speed n	600 min^{-1}	1000 min^{-1}

The simulation is basically performed for two sets of process parameters, being embraced in Table 2, one of which the experimental test weld is referred to as set A. In Figure 5 and 6 a comparison between the test weld and the simulation results is given. A qualitative agreement of the flash formation can be identified.

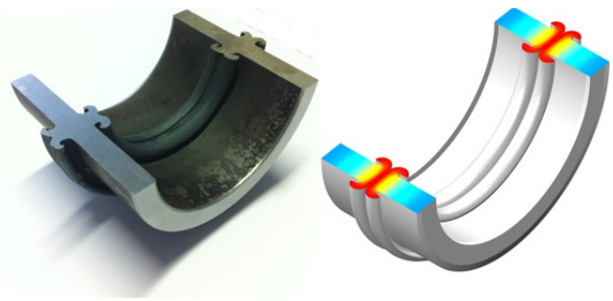

Figure 5: The test weld in reality and simulation.

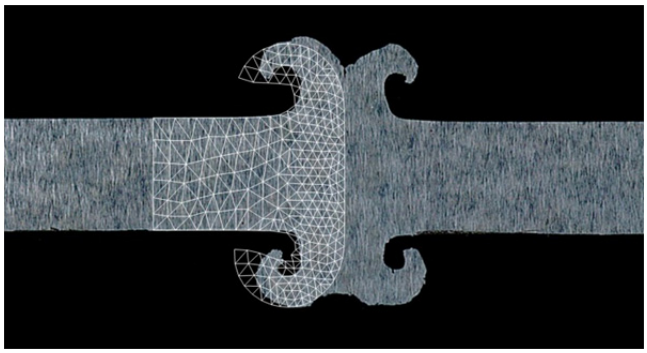

Figure 6: Comparison of flash geometry between simulation and experiment.

Figure 7 illustrates the twist during the simulation of the friction welding process. The support of the twist degree of freedom in conjunction with the regularized friction law of eq. (8) allows for a steady transition from surface friction into plastic friction during the simulation.

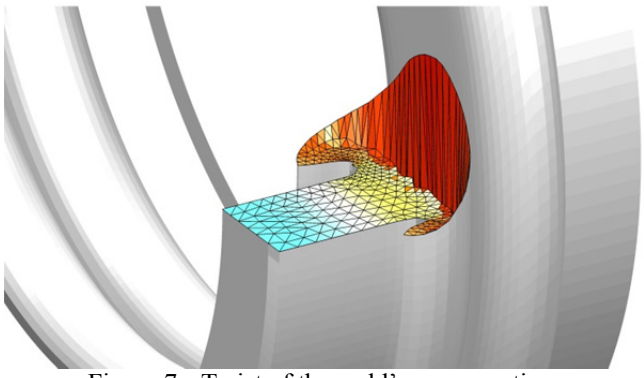

Figure 7: Twist of the weld's cross-section.

The influence of the process parameter is highlighted when comparing the simulation results of parameter set A and B with each other. As it can be seen in Figure 8, the dimension of the flash significantly depends on the time of the welding. Set A represents a slow process where due to the lower rotary speed the rubbing stage needs to be quite long in order to create the necessary heat input. The result is a much wider shape of the flash than for the simulation with parameter set B, where a fast rotary speed and a short rubbing time is given. With the aid of the presented model, energy profiles as displayed in Figure 9 can be obtained. Therein it is seen that at the end of the rubbing stage an increasing part of heat energy is generated by plastic dissipation. On the other hand the amount of heat power can be directly compared to cooling power, revealing that for this is example the cooling hardly enters the process since it is of very small magnitude.

Of crucial interest when modeling RFW is the prediction of the upset of the weld. In Figure 10a and 10b the rotary speed of parameter set A is altered, while leaving all other parameters unaffected. It is nicely seen that for rotary speeds below 400 min^{-1} no significant upset is gained anymore, being reasoned by the insufficient heat input.

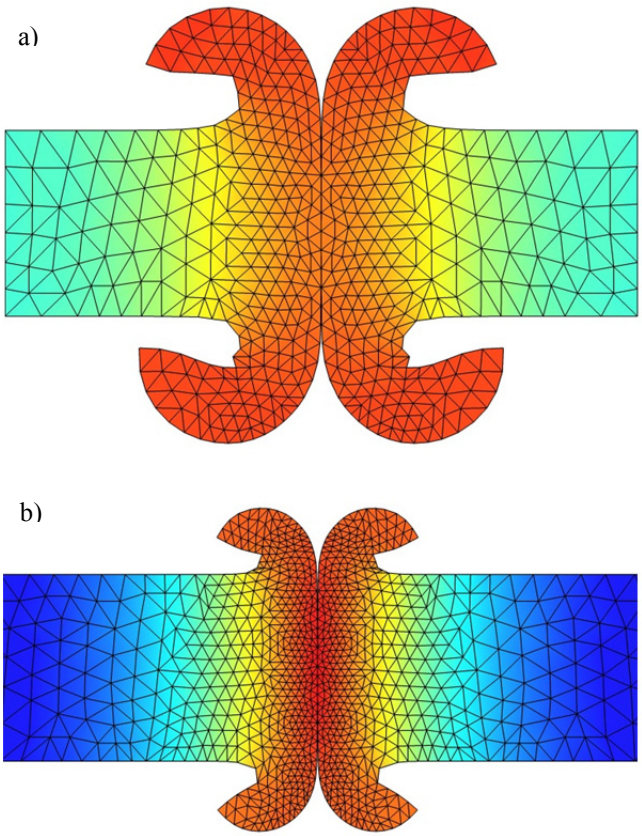

Figure 8: Flash comparison for the simulation with parameter set A (8a) and parameter set B (8b).

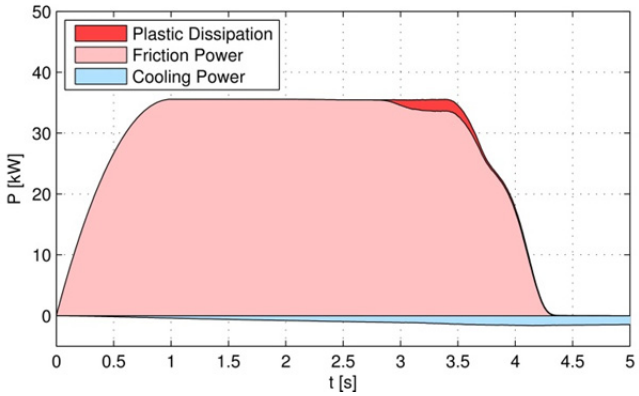

Figure 9: Energy profile for the process simulation on basis of parameter set B.

On the contrary above the region of 480 min^{-1} the final upset turns out to be linear dependent on the rotary speed. Another essential insight is achieved when looking at the maximum temperatures during the same variation of parameters, being displayed in Figure 11. Apparently, the melting temperature is not exceeded for none of the underlying welding settings. Instead, rather a saturation of maximum temperature is identified when increasing the rotary speed, which is in accordance with the well accepted statement that during friction welding the liquid phase is generally not reachable [17].

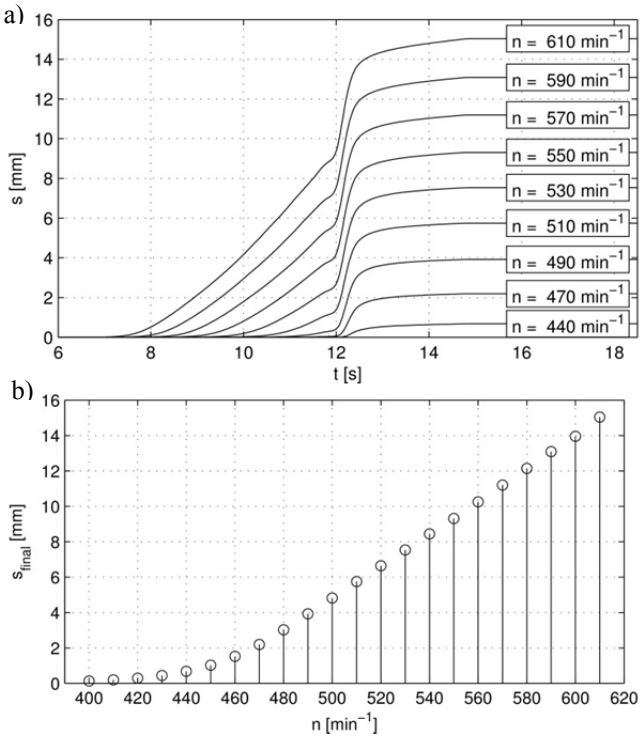

Figure 10: Influence of an altering rotary speed on the axial feed timelines (10a) and the weld's total upset (10b) employing parameter set A.

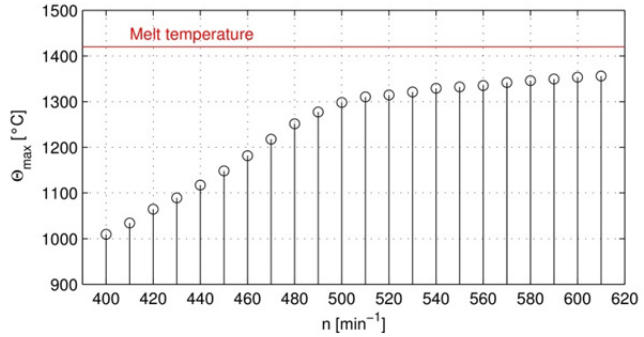

Figure 11: Maximum temperature during welding as a function of the rotary speed of parameter set A.

Conclusion

The present contribution demonstrates the performance and potentials of a new friction welding modeling approach being implemented by an in-house Matlab code called *virtua RFW*. Main focus in this regard is the posed Carreau fluid law, which is capable of estimating the plastic flow during the rubbing and forging phase of the process on the basis of easy accessible parameters like the yield limit at room temperature and the melting temperature. It has been demonstrated that the simulation results are in qualitative agreement with the experiments. One of the most important applications of the model is the study of process parameter dependencies like the influence of the rotary speed on the final upset. Moreover, it is shown that with the aid of the implemented material law a very robust and stable simula-

tion is feasible, with computation times generally less than one hour per simulation. Future work will be the extension of the model to dissimilar weld partners. Furthermore, a staged simulation is favored in which the cooling phase is modeled by a small deformation CSM-material law in order to determine the residual stresses of the weld.

Acknowledgements

The authors would like to thank the Federal State of Saxony-Anhalt, Germany for its support.

References

[1] C. Agelet de Saracibar, M. Chiumenti, D. Santiago, M. Cervera, N. Dialami, and G. Lombera. A computational model for the numerical simulation of fsw processes. *AIP Conference Proceedings*, 1252(1):81–88, 2010.

[2] P.J. Carreau. Rheological equations from molecular network theories. *Transactions of the Society of Rheology*, 16(1):99–127, 1972.

[3] Y. Chao and X. Qi. Heat transfer in friction stir welding—experimental and numerical studies. *Transactions of the ASME*, 125:138–145, 2003.

[4] M. Chiumenti, M. Cervera, C.A. Saracibar, and N. Dialami. Numerical modeling of friction stir welding processes. *Computer Methods in Applied Mechanics and Engineering*, 1:1–45, 2012.

[5] V.R. Davé, M.J. Cola, and G.N.A. Hussen. Heat generation in the inertia welding of dissimilar tubes. *Welding Journal*, pages 246S–252S, 2001.

[6] DIN EN ISO 15620. Reibschweißen von metallischen Werkstoffen. *Deutsches Institut für Normung*, 2000.

[7] DVS Merkblatt 2909. Reibschweißen von metallischen Werkstoffen. *Deutscher Verband für Schweißen und verwandte Verfahren e.V.*, 2009.

[8] F. Garofalo. *Fundamentals of creep and creep-rupture*. Macmillan, New York, 1965.

[9] H. Giesekus. *Phänomenologische Rheologie - Eine Einführung*. Springer-Verlag, 1994.

[10] B. Grant, M. Preuss, P.J. Withers, G. Baxter, and M. Rowlson. Finite element process modelling of inertia friction welding advanced nickel-based superalloy. *Materials Science and Engineering: A*, 513 - 514(0):366 – 375, 2009.

[11] R. Hamilton, D. MacKenzie, and H. Li. Multi-physics simulation of friction stir welding process. *Engineering Computations*, 27:967–985, 2010.

[12] J. Hilgert. *Knowledge Based Process Development of Bobbin Tool Friction Stir Welding*. PhD thesis, Technischen Universität Hamburg-Harburg, 2012.

[13] G.R. Johnson and W.H. Cook. A constitutive model and data for metals subjected to large strains, high strain rates and high temperatures. *Proceedings of the 7th International Symposium on Ballistics*, page 541–547, 1983.

[14] M. Maalekian. Thermal modeling of friction welding. *ISIJ International*, 48(10):1429–1433, 2008.

[15] A. Moal and E. Massoni. Finite element simulation of the inertia welding of two similar parts. *Engineering Computations*, 12:497–512, 1995.

[16] D. H. Santiago, G. Lombera, S. Urquiza, A. Cassanelli, and L. A. Vedia. Numerical modeling of welded joints by the "friction stir welding" process. *Materials Research*, 7:569–574, 2004.

[17] G. Schäfer, A. Dietzel, D. Schober, and S. Buchholz. *Handbuch Reibschweiszen*. VVB Getriebe und Kupplungen, 1976.

[18] H.N.B. Schmidt and J. H. Hattel. A local model for the thermomechanical conditions in friction stir welding. *Modelling and Simulation in Materials Science and Engineering*, 13:77–93, 2005.

[19] L. Wang, M. Preuss, P.J. Withers, G. Baxter, and P. Wilson. Energy-input-based finite-element process modeling of inertia welding. *Metallurgical and Materials Transactions B*, 36:513–523, 2005.

[20] H. S. Yu, G. T. Houlsby, and H. J. Burd. A novel isoparametric finite element displacement formulation for axisymmetric analysis of nearly incompressible materials. *International Journal for Numerical Methods in Engineering*, 36(14):2453–2472, 1993.

[21] B. Zhang and T.N. Baker. Effect of the heat treatment on the hot deformation behaviour of AA6082 alloy. *Journal of Materials Processing Technology*, 153-154:881–885, 2004.